Journal of Solid State Chemistry 300 (2021) 122238

Contents lists available at ScienceDirect

Journal of Solid State Chemistry

journal homepage: www.elsevier.com/locate/jssc

Preparation of a hollow HZSM-5 zeolite supported molybdenum catalyst by desilication-recrystallization for enhanced catalytic properties in propane aromatization

Guohao Xu, Peng Zhang, Junjun Cheng, Ting Wei, Xuedong Zhu [*], Fan Yang

Engineering Research Center of Large-Scale Reactor Engineering and Technology, Ministry of Education, East China University of Science & Technology, Shanghai, 200237, PR China

ARTICLE INFO

Keywords:
Propane aromatization
Desilication-recrystallization
Hollow Mo/HZSM-5
Silicon-rich external surface

ABSTRACT

A hollow HZSM-5 supported molybdenum (Mo) catalyst was successfully prepared by desilication-recrystallization method of HZSM-5 in tetrapropylammonium hydroxide (TPAOH) solution. The as-synthesized catalyst exhibiting excellent performance in propane aromatization reaction was thoroughly investigated, along with the mechanism for the formation of hollow structure and mechanism for the deactivation. Results revealed that TPA $^{+}$ exerted a controllable desilication and recrystallization effect. Compared with Na_2CO_3 treatment which led to a mesoporous structure, TPAOH treatment was able to leach out the inner Si species by OH^- and then those Si species recrystallized on the external surface, resulting in the hollow structure and a silicon-rich external surface. In addition, the hollow zeolite exposing higher external surface provided more anchoring sites for Mo species, which was beneficial to the Mo related Lewis acid sites but decreased the surface Bronsted acidity. At 823 K and a space velocity of 1800 $mL \cdot g^{-1} \cdot h^{-1}$, the hollow Mo/HZSM-5(TPAOH) catalyst behaved a propane conversion of 73.01% and aromatics selectivity of 77.36%, exceeding those of the hierarchical Mo/HZSM-5(Na_2CO_3) catalyst by 5.97% and 9.96%, respectively. These features of Mo/HZSM-5(TPAOH) granted it superb diffusion ability and optimized Bronsted/Lewis acid ratio ($B/L = 1.3$), which greatly enhanced the propane conversion and aromatic selectivity together with a preeminent catalytic stability.

1. Introduction

Direct catalytic conversion of propane into aromatics has become an important research topic due to the growing demand for aromatics [1,2]. Commercially, propane aromatization utilizing bifunctional catalysts such as MFI type zeolite supported metal species was named “Cyclar”, which was developed jointly by Universal Oil Products Company (UOP) and British Petroleum (BP) [1]. Different metals (e.g., Zn, Pt and Ga) have been impregnated to improve the catalytic performance in propane aromatization[3–5], however, few attempts about Mo were made. It is well-known that Mo-containing catalysts have been widely applied in methane aromatization [6]. Thus, studying the influence of Mo on the propane aromatization reaction will be conducive to intensively understand the aromatization of lower alkanes, especially the mixed aromatization of methane and propane, which will give some inspiration to the industrialization development of low-carbon alkanes.

In addition to metal modification [7–9], the topology of zeolite is also critical to the aromatization of propane. The diameter of micropores (0.51–0.55 nm, 0.53–0.56 nm) within the MFI topology of ZSM-5 zeolite matches well with the kinetic diameters of some aromatics, leading to excellent selectivity towards the desired products. Yet, the excellent shape selectivity caused by the sizes of micropores also bring non-negligible diffusion resistence, leading to the blockage of channels and pores by coking [10]. In order to improve the mass transport of larger reactants [11], researchers resort to ameliorating the diffusion capability of the micropore materials by introducing mesopores and reducing the crystal sizes [12,13]. Among those methods, reprocessing of ZSM-5 zeolite to introduce mesopores has acquired lots of attention because of the feasibility and low-cost nature, making it a promising way in industry [14,15]. One of the reprocessing strategy, rather popular in application, is dealumination with acid solution and desilication with alkaline solution, among which desilication generates mesopores easily, and hence is widely applied in the preparation of hierarchical ZSM-5 zeolite [16].

---

[*] Corresponding author.
E-mail address: xdzhu@ecust.edu.cn (X. Zhu).

https://doi.org/10.1016/j.jssc.2021.122238
Received 7 March 2021; Received in revised form 14 April 2021; Accepted 27 April 2021

However, one disadvantage is that alkali treatment can also lead to the formation of a large amount of amorphous substances in the reaction, blocking the pores and reducing the crystallinity of ZSM-5 and then affect the performance of the catalyst [10]. To overcome this shortcomings, Li et al. [17] synthesized a series of the hollow ZSM-5 zeolite by desilication-recrystallization of silicalite-1. It was proposed that the hollow ZSM-5 zeolite with high crystallinity further shortened its micropore length and greatly improving the stability of methanol to hydrocarbons reaction. Guo et al. [15] synthesized hollow zeolite by desilication-recrystallization of silicalite-1 in TPAOH solution. The hollow structure increased CO_2 conversion and $C5^+$ higher hydrocarbons in the hydrogenation of CO_2 to hydrocarbons.

Inspired by these interesting studies, introducing hollow structure and employing Mo impregnation is expected to effectively enhance catalytic performances in propane aromatization. To explore the mechanism for the evolution of hollow structure, a parent HZSM-5 treated with the conventional alkali (Na_2CO_3) solution was used as a comparison, and the physicochemical properties of the catalyst and the catalytic performance of propane aromatization reaction were investigated.

2. Experimental

2.1. Raw materials

All raw materials were of analytical grade and did not require further purification. The parent HZSM-5 zeolite (SiO_2/Al_2O_3 ratio = 36, abbreviated as HZSM-5(0) in the following) was supplied by the Tianjin Nanhua Catalyst Co., Ltd., Tianjin, China. Sodium carbonate (Na_2CO_3) and ammonium chloride (NH_4Cl) were purchased from Heraeus Compan, Hanau, Germany. Tetrapropylammonium hydroxide (TPAOH) was purchased from Shanghai Dibo Chemical Technology Co., Ltd., Shanghai, China. Ammonium heptamolybdate ($(NH_4)_6Mo_7O_{24}\cdot 4H_2O$) was provided by Shanghai Macklin Biochemical Technology Co., Ltd., Shanghai, China.

2.2. Preparation of catalyst

The hollow ZSM-5 zeolites with silicon-rich exterior surface were synthesized according to a previous work [18]. HZSM-5(0) was placed in 0.3 M TPAOH solution, stirred for at 353 K 6 h, and then transferred into a Teflon-lined steel autoclave for crystallization at 443 K for 36 h, followed immediately by washing with distilled water, filtering, drying at 393 K for 12 h and calcining at 823 K for 4 h. The as-prepared sample was remarked as HZSM-5(TPAOH).

For comparison, HZSM-5(0) was placed in 0.6 M Na_2CO_3 solution, stirred in a water bath at 353 K for 6 h, followed immediately by washing with distilled water, filtering, drying at 393 K for 12 h and calcining at 823 K for 4 h. The H-form sample was obtained after ion exchanged with 1 M NH_4Cl solution at 353 K for 2h (three times), followed immediately by washing with distilled water, filtering, drying at 393 K for 12 h and calcining at 823 K for 4 h to remove NH_4^+. The obtained sample was termed as HZSM-5(Na_2CO_3).

Mo-containing catalysts (Mo wt% = 6%) were synthesized by incipient wet impregnation with $(NH_4)_6Mo_7O_{24}\cdot 4H_2O$ solution. After impregnation, the samples were dried overnight at 353 K, and then calcined at 823 K for 4 h to obtain Mo/HZSM-5(0), Mo/HZSM-5(TPAOH) and Mo/HZSM-5(Na_2CO_3) catalysts.

2.3. Catalyst characterization

X-ray diffraction (XRD) patterns were carried out on a RIGAKU diffractometric using CuKα radiation with a scanning speed 8°/min and the step size of 0.02°. X-ray photoelectron spectroscopy (XPS) and in situ Ar ionic sputtered HZSM-5(TPAOH) were measured using an ESCALAB 250 spectrometer, operating at 1486.6 eV monochromatic AlKα source as well as 14 kV and 30 mA. The analyzed area was 3000 Å in diameter and Ar ionic sputtering was performed with a beam energy of 4 keV and a sputtering rate of 25 Å/min. The sputtered sample was remarked as HZSM-5(TPAOH)-S. Magic angle spinning (MAS) ^{27}Al single pulse NMR spectra were recorded on a Bruker Avance DMX-500 NMR spectrometer equipped with a 2.5 mm MAS probe head operating at an ^{27}Al NMR resonance frequency of 130.3 MHz. Nitrogen adsorption/desorption was recorded on a Micromeritics ASAP-2020V3.00H analyzer [19]. All samples were outgassed at 453 K for 12 h under vacuum to remove moisture and volatile impurities before the measurements. Corresponding isotherms were measured at −77 K. Al and Mo contents were quantitatively analyzed by inductively coupled plasma atomic emission spectrometer (ICP-AES) manufactured in Agilent, USA. Transmission electron microscopy (TEM) micrographs were measured with a JEM-1400 transmission electron microscope operating at 200 kV. Infrared spectra of pyridine adsorption (Py-IR) and OH stretching regions of the IR spectra were carried out on a Nicolet iS50 spectrometer with 32 scans at an effective resolution of 4 cm^{-1}. The quantification of acid sites was performed using the same expressions as reported by Emeis [20]. The carbon deposits from the as-used catalysts were determined using an PerkinElmer TGA 8000. Samples were heated in uncovered alumina crucibles at a rate of 10 K/min to 973 K in air atmosphere.

2.4. Catalyst evaluation

The activities of the propane aromatization reaction were evaluated in a small fixed-bed quartz tube reactor with 0.3 g of 20–40 mesh sample. The sample was located between two quartz wool plugs and heated to 823 K under N_2 flow (15 mL min^{-1}). After temperature equilibration was achieved at 823 K, the gaseous feed (consisting of 60 vol% C_3H_8 and 40 vol% N_2) was passed into the catalyst bed at a space velocity of 1800 $mL\cdot g^{-1}\cdot h^{-1}$ and atmospheric pressure. Using N_2 as an internal standard for analyzing products, the products were analyzed on-line with a gas chromatograph (GC). The gaseous phase products monitored by online analysis using TDX-01 packed column equipped with a TCD detector and a PLOT-Q pillared column connected to an FID detector produced by Shimadzu. Aromatic hydrocarbons were analyzed with an FID detector on a DB-WAX column produced by Agilent. The propane conversion $x_{propane}$ and product selectivity S_i were calculated in the following equations.

$$x_{propane} = \frac{C_{propane}(in) - C_{propane}(out)}{C_{propane}(out)} \times 100 \tag{1}$$

$$S_i = \frac{C_i}{\Sigma(C_i) - C_{propane}(\mathrm{out})} \times 100 \tag{2}$$

where C_i and $C_{propane}$ are the concentrations for species i and propane, respectively.

3. Results and discussion

3.1. Catalytic characterization

3.1.1. X-ray diffraction (XRD)

The X-ray diffraction patterns and the relative crystallinities of the synthesized samples are depicted in Fig. 1. Characteristic diffraction peaks of these samples exhibited at 2θ = 7.9°, 8.8°, 23.1°, 23.7° and 24.4°, which indicated that HZSM-5(0) treated with TPAOH and Na_2CO_3 solutions still retained the MFI structure. To obtain the relative crystallinity of the modified samples, HZSM-5(0) was selected as the reference and regarded its crystallinity as 100%. By calculating the ratio of the five characteristic peak areas of the modified samples relative to the parent HZSM-5(0), the relative crystallinity of HZSM-5(Na_2CO_3) and HZSM-5(TPAOH) were obtained. It can be seen that the relative crystallinity of HZSM-5(Na_2CO_3) was only 69%, revealing a serious destruction of the zeolite. The Si species of HZSM-5(0) were etched by OH^-, which caused a

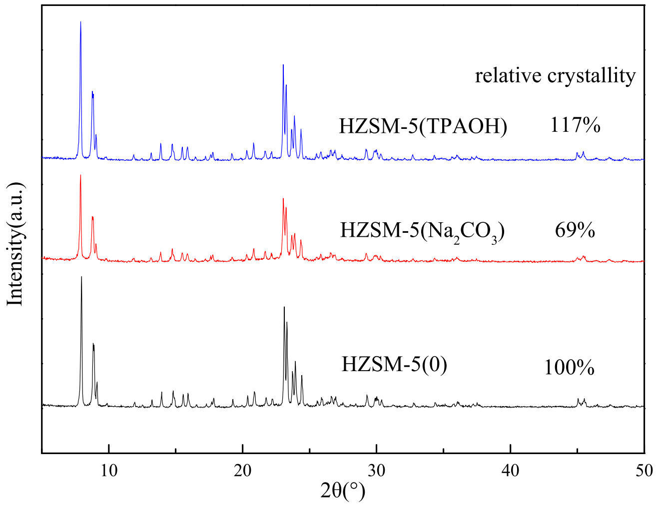

Fig. 1. XRD patterns of the synthesized samples.

corrosion of framework structure [21], resulting in a decrease in the crystallinity of HZSM-5(Na_2CO_3). It was interesting that the relative crystallinity of HZSM-5(TPAOH) increased rather than decreased. As reported, with the help of TPA^+, some of inner Si species of HZSM-5(0) etched by OH^- moved back to the surface of zeolite and then went through a secondary crystallization [11,22]. Therefore, compared with the relative crystallinity of HZSM-5(0) and HZSM-5(Na_2CO_3), the relative crystallinity of HZSM-5(TPAOH) increased.

3.1.2. X-ray photoelectron spectroscopy (XPS)

The surface molar composition and the chemical environments of Al and Si of HZSM-5(0), HZSM-5(Na_2CO_3), HZSM-5(TPAOH) and HZSM-5(TPAOH)-S are depicted in Table 1 and Fig. 2, respectively. It was clear that the surface Al species of HZSM-5(TPAOH) were not detected. After Ar ion sputtering, the silicon-rich shell surface was removed, and Al species of HZSM-5(TPAOH)-S were detected again, which further demonstrated that some of inner Si species of HZSM-5(0) were etched by OH^- and the leached Si species were then recrystallized on the external surface of zeolite, while the Al-rich part of the zeolite framework remained intact by the strong repulsion effect between AlO_4^- and OH^- groups [23]. Such a process generated a silicon-rich surface [24]. Compared with HZSM-5(0), there was a decrease in the surface Si species proportion of HZSM-5(Na_2CO_3), which occurred in parallel with an increase in the proportion of Al species. This phenomenon was caused by the fact that OH^- mainly etched the surface Si species, which in turn increased the surface Al species proportion [10].

3.1.3. OH stretching regions of the IR spectra

The OH stretching regions of the IR spectra of the above samples are shown in Fig. 3. The three main bands on above samples are assigned to bridged hydroxyl groups (Si(OH)Al, 3610 cm^{-1}), extra-framework aluminum species (3665 cm^{-1}), and silanol groups (3735-3740 cm^{-1}). Compared with the IR spectra of HZSM-5(0), the decrease of bridged hydroxyl groups and the increase of extra-framework aluminum species on HZSM-5(Na_2CO_3) implied that the structure of HZSM-5(0) was etched by OH^-, some framework Al species were transformed into extra-framework Al species in the erosion process [25]. Comparison of the spectra of HZSM-5(0) and HZSM-5(TPAOH) showed that HZSM-5(TPAOH) contained much more silanol groups, indicating that HZSM-5(TPAOH) possessed the silicon-rich external surface [26]. This was in accordance with the result about the formation of the silicon-rich external surface obtained from XPS.

Table 1
Surface molar composition of the synthesized samples.

Sample	Surface(XPS)
HZSM-5(0)	$Si_{93}Al_7$
HZSM-5(Na_2CO_3)	$Si_{88}Al_{12}$
HZSM-5(TPAOH)	$Si_{100}Al_0$
HZSM-5(TPAOH)-S	$Si_{97}Al_3$

3.1.4. ^{27}Al MAS NMR spectroscopy

The Al distribution in the synthesized samples was investigated by ^{27}Al MAS NMR spectroscopy (Fig. 4). The spectra contain four bands at chemical shifts of −11 ppm, 0 ppm, 14 ppm and 55 ppm. The peak around 55 ppm is due to framework Al (FAl). The feature at 0 ppm originates from extraframework Al (EFAl) in octahedral coordination [27]. The signals at −11 and 14 ppm are due to $Al_2(MoO_4)_3$, which also belonged to the EFAl phase. In HZSM-5(0), Al was predominantly present as FAl. Modification of HZSM-5(0) with Mo led to a decrease of the FAl signal caused by the proximity of cationic Mo-oxo complexes that replaced the protons [28]. The increasing amount of $Al_2(MoO_4)_3$ in Mo/HZSM-5(Na_2CO_3) was related to FAl damage occurring during the alkali treatment, which further confirmed that the skeleton structure of Mo/HZSM-5(Na_2CO_3) was deeply damaged.

3.1.5. Texture properties

The pore structure data and the nitrogen physisorption isotherms of the synthesized samples are depicted in Table 2 and Fig. 5, respectively. When the p/p_0 was 0.44–0.97, obvious hysteresis loops were apparent, indicating that mesopores were successfully introduced into the zeolite and the micro-mesoporous hierarchical structure was formed. More interestingly, compared with the hierarchy factor (HF) of HZSM-5(0), the hierarchy factor of HZSM-5(TPAOH) and HZSM-5(Na_2CO_3) decreased rather than increased [11], demonstrating that the samples were more severely treated (higher alkalinity), the HF lowered due to the relatively strong decrease of the micropore volume [23]. Comparing the hysteresis loops, it can be found that the hierarchical HZSM-5(Na_2CO_3) exhibited much higher mesoporosity than HZSM-5(TPAOH) and HZSM-5(0), further confirming that the desilication degree of HZSM-5(Na_2CO_3) was more serious. In addition, HZSM-5(Na_2CO_3) had a larger total pore volume of 0.32 $cm^3\ g^{-1}$ but a lower microporous surface area of 151 $m^2\ g^{-1}$, which suggested that some amorphous substances produced during the process of desilication remained in the microporous channels, reducing the microporous surface area [29]. Compared with the pore structure properties of HZSM-5(0), HZSM-5(TPAOH) showed a little lower microporous surface area (S_{micro} = 172 $m^2\ g^{-1}$) and a higher mesoporous volume (V_{meso} = 0.19 $cm^3\ g^{-1}$), indicating that mesopores were generated by consuming microporous structure [14]. Comparing the external specific surface area of these samples before and after impregnation with Mo, it was found that the external specific surface area of these samples were significantly reduced after impregnation with Mo, indicating that Mo species mainly located on the external surface of zeolite [30]. Table 2 lists the Mo and Al contents. It was found that the content of Al decreased with an increase of Mo content. This suggested that the a portion of Al species was replaced by Mo species [31]. This trend was in agreement with the work carried out by Christiaan H.L. Tempelman et al. [28]. In addition, the observation that the Mo content of Mo/HZSM-5(TPAOH) was higher than that of Mo/HZSM-5(Na_2CO_3) may be explained by the fact that HZSM-5(TPAOH) possessed the higher external surface area (S_{meso} = 160 $m^2\ g^{-1}$), which provided more loading sites for Mo species [32].

3.1.6. Transmission electron microscope (TEM)

Fig. 6 presents the TEM images of these samples. Mo/HZSM-5(0) had regular crystal morphology with dimensions of 4 μm × 1.6 μm (Fig. 6a). Mo/HZSM-5(Na_2CO_3) had an irregular external topography with a large irregular void in the interior, indicating that Mo/HZSM-5(0) was severely corroded by OH^-. After the desilication-recrystallization of zeolite, a regular hollow structure was observed in Mo/HZSM-5(TPAOH)

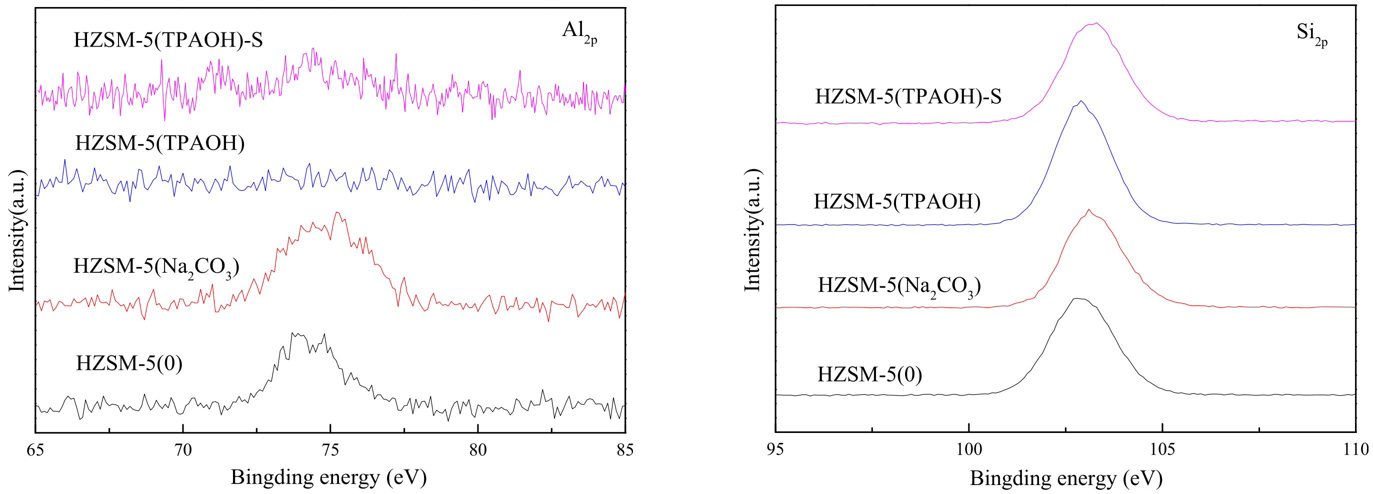

Fig. 2. Al_{2p} and Si_{2p} XPS spectrogram of the synthesized samples.

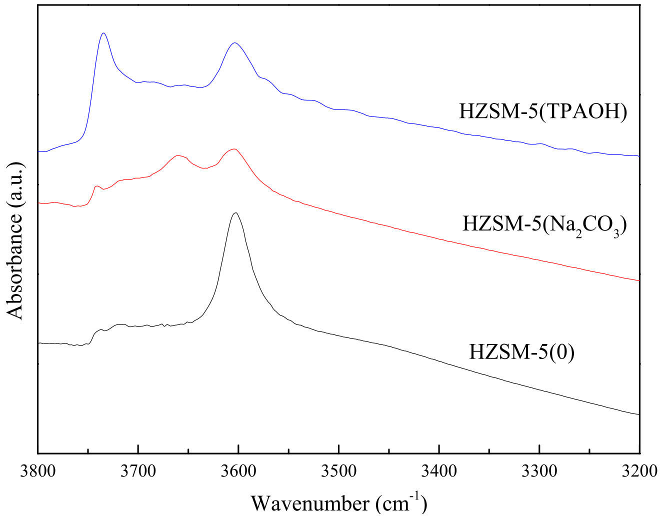

Fig. 3. OH stretching regions of the IR spectra of the synthesized samples.

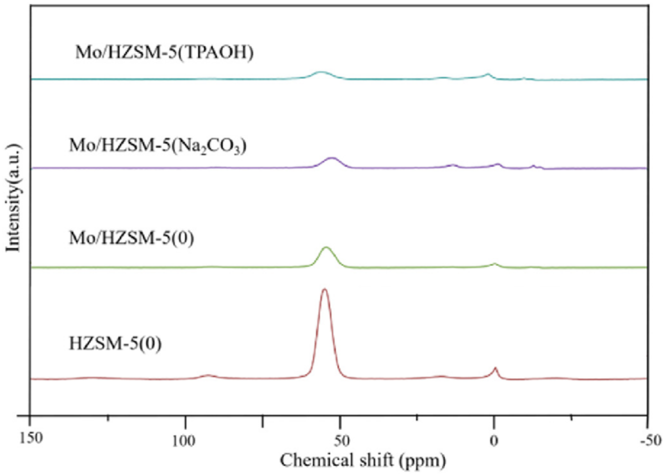

Fig. 4. ^{27}Al MAS NMR spectra of the synthesized samples.

(Fig. 6c). During the process of desilication-recrystallization, TPA^+ was partly adsorbed on the external surface of HZSM-5(0) and protected the external Si species from being etched while the inner Si species were easily leached out by OH^{-15}, [33]. The leached Si species quickly diffused out of zeolite and then recrystallized to generate a silicon-rich external surface of zeolite [34]. These variations of ZSM-5 structure were also in good accordance with XRD and XPS results.

On the basis of the above analysis, the fabrication mechanism of the alkali treatment and desilication-recrystallization of HZSM-5(0) are illustrated in Scheme 1. When HZSM-5(0) is used as the parent, TPA^+ is mainly adsorbed on the surface of HZSM-5(0) via electrostatic interactions [22]. In the process of desilication, TPA^+ can not get into the interior of HZSM-5(0) due to its large molecular size, which protects the surface of the crystal from being etched [35]. Consequently, the inner Si species are removed by OH^-, resulting in the formation of mesopores. In addition, under the template of TPA^+, HZSM-5(TPAOH) with a silicon-rich external surface is formed by the leached Si species recrystallizated on the external surface [22] (Scheme 1a). During this continuous desilication-recrystallization process, the regular hollow structure is produced. Comparatively, without of the protective effect from TPA^+, OH^- makes it easy to etch Si species unselectively, resulting in the change of the morphology of zeolite and a large irregular void in the interior (Scheme 1b).

3.1.7. Acid properties

Fig. 7 illustrates the Py-IR spectra of the above samples after chemisorbed pyridine and evacuation at 423 K. The infrared bands used to separately quantify the Brønsted acid sites and the Lewis acid sites were the peaks at 1540 and 1450 cm^{-1}, respectively. A comparison of acid concentrations of HZSM-5(0) and Mo/HZSM-5(0) revealed that Brønsted acid concentration decreased in parallel with an increase in Lewis acid concentration upon introduction of Mo, indicating that Mo-Lewis acid was formed by consuming the Brønsted acid [36]. Compared with Mo/HZSM-5(0), an increase in Brønsted acid sites of Mo/HZSM-5(Na_2CO_3) was a result of Si leaching from the framework, making more acid site accessible to pyridine (Table 3). Compared with Mo/HZSM-5(0), the concentration of Brønsted acid sites of Mo/HZSM-5(TPAOH) decreased, whereas the concentration of Lewis acid sites increased. The reason can be explained by the fact that Mo/HZSM-5(TPAOH) possessed a larger amount of Mo, and more Mo-Lewis acid were generated by consuming the Brønsted acid [32], which was in consistent with the observation from the ICP. In addition, with the help of TPA^+, the leached Si species formed the external surface skeleton structure of zeolite, also resulting in a decrease in the concentration of Brønsted acid. It was worth mentioning that Mo/HZSM-5(TPAOH) possessed the lowest Brønsted/Lewis acid ratio ($B/L = 1.3$), which was supposed to be ascribed to the synergistic effect of the larger amount of Mo-Lewis acid and the Si-rich external surface.

Table 2
Textural properties of the synthesized samples.

Sample	S_{BET}/(m [2]·g^{-1})	S_{micro}/(m [2]·g^{-1})	S_{ext}/(m [2]·g^{-1})	V_{total}/(cm [3]·g^{-1})	V_{meso}/(cm [3]·g^{-1})	Hierarchy Factor[a]	Al (wt%)[b]	Mo (wt%)[b]
HZSM-5(0)	319	188	131	0.25	0.14	0.181	2.2	–
HZSM-5(Na_2CO_3)	286	151	135	0.32	0.23	0.133	2.2	–
HZSM-5(TPAOH)	332	172	160	0.28	0.19	0.155	2.2	–
Mo/HZSM-5(0)	298	196	102	0.23	0.12	0.164	1.8	4.7
Mo/HZSM-5(Na_2CO_3)	278	162	116	0.31	0.22	0.121	1.9	4.4
Mo/HZSM-5(TPAOH)	310	184	126	0.25	0.18	0.130	1.6	5.3

[a] Hierarchy factor = (V_{micro}/V_{total}) × (S_{ext}/S_{BET}); V_{micro} = V_{Total}-V_{meso}.
[b] The values of metal loading were determined by ICP-AES analysis.

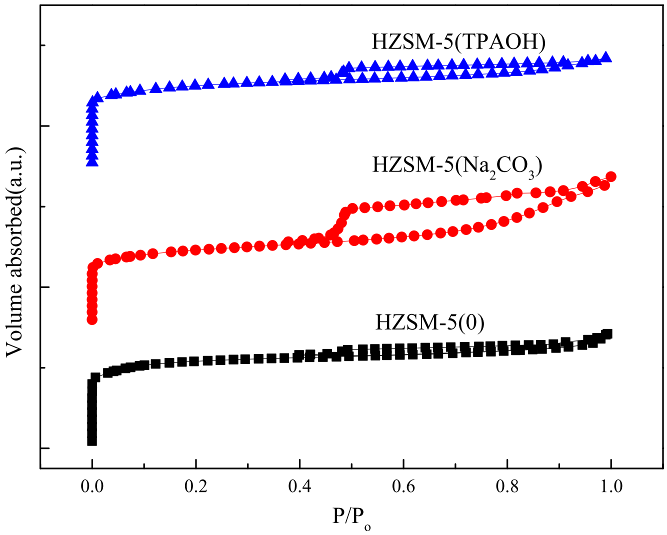

Fig. 5. N_2 physisorption isotherms of the synthesized samples.

3.2. *Catalytic reactions*

3.2.1. *Catalytic performance of the synthesized catalysts*

The product distribution and yield of these catalysts in propane aromatization are listed in Table 4 and Fig. 8, respectively. To investigate the effect of Mo sites on the reaction, HZSM-5(0) without Mo loading was used as the comparison. Compared with Mo/HZSM-5(0), the propane conversion and gas phase product yield of HZSM-5(0) were significantly lower, especially the yield of propene, demonstrating that Mo sites can promote the dehydrogenation of propane to generate propene.

In order to compare the catalytic performance of Mo/HZSM-5(TPAOH), Mo/HZSM-5(Na_2CO_3) with the same 6 wt% Mo loading were prepared. Compared with Mo/HZSM-5(Na_2CO_3), Mo/HZSM-5(TPAOH) exhibited superior propane conversion of 73.01% and aromatics selectivity of 77.36%, which were higher than those of Mo/HZSM-5(Na_2CO_3) by 5.97% and 9.96%, respectively. In addition, the gas phase yield of Mo/HZSM-5(TPAOH) was lower, whereas the liquid phase yield was much higher than that of Mo/HZSM-5(Na_2CO_3), demonstrating that the hollow structure was conducive to generate aromatics through the rapid transfer of light hydrocarbons.

The reaction sequence of propane aromatization involves the dehydrogenation of propane on the Lewis acid sites and Mo sites, and the cracking of propane on the Bronsted acid sites, which subsequently oligomerizes and cyclizes on the Bronsted acid sites, and then dehydrogenates on the Lewis acid sites to aromatics [37] (Scheme 2). Therefore, Bronsted acid sites and Lewis acid sites are indispensable for propane aromatization [38]. However, the high amount of Bronsted acid is easy to promote the secondary reactions of benzene, thereby deactivating the catalyst, because the formed benzene readily react to become poly-aromatics and coke [39]. Consequently, the higher Lewis acid and the lower Brønsted acid are beneficial to the aromatization of propane. Whereas, the lower Lewis acid concentration (72.7 μmol g^{-1}) of Mo/HZSM-5(Na_2CO_3) was inadequate for propane conversion and the pore structure blocked by the removed amorphous silicon species was not conducive to the diffusion of the product, reducing the conversion of propane. Furthermore, the higher Brønsted acid (196.9 μmol g^{-1}) of Mo/HZSM-5(Na_2CO_3) led to the formation of poly-aromatics and coke, reducing the selectivity of aromatics. In contrast, the higher Lewis acid concentration (123.5 μmol g^{-1}) of Mo/HZSM-5(TPAOH) facilitated the activation of propane. The hollow structured Mo/HZSM-5(TPAOH) was conductive to shorten the diffusion path, which can facilitate quick diffusion of desired products out of the intraframework channels and in turn accelerate the reaction [40]. In addition, Mo/HZSM-5(TPAOH) with the silicon-rich external surface possessed a higher external surface area [18], which provided more loading sites for Mo species to generate the Mo-Lewis acid and decreased the concentration of Brønsted acid, suppressing the side reactions and improving the aromatics selectivity. As a consequence, Mo/HZSM-5(TPAOH) exhibited the higher propane conversion and aromatics selectivity than Mo/HZSM-5(Na_2CO_3).

Compared with the catalytic performance of Mo/HZSM-5(0), Mo/HZSM-5(Na_2CO_3) had the higher propane conversion, which was attributed to its micro-mesoporous hierarchical structure, thereby improving mass transfer performance [35]. Owing to the higher Bronsted acid amount, the aromatics produced during the aromatization process

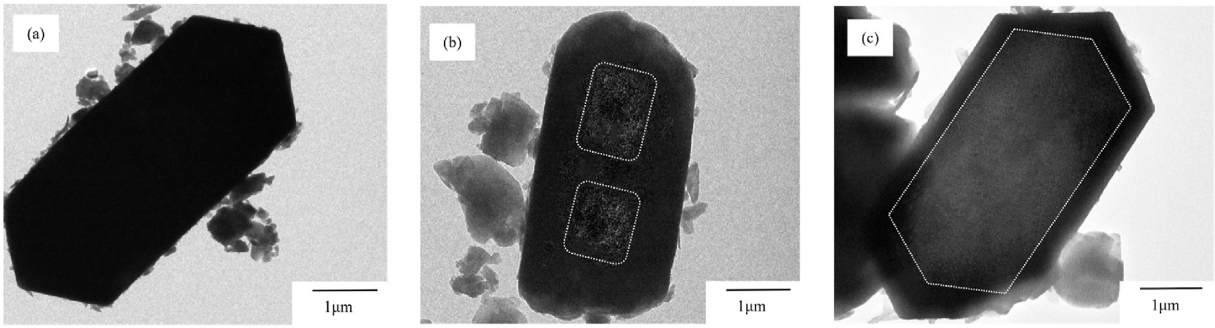

Fig. 6. Typical TEM images of (a) Mo/HZSM-5(0), (b) Mo/HZSM-5(Na_2CO_3) and (c) Mo/HZSM-5(TPAOH).

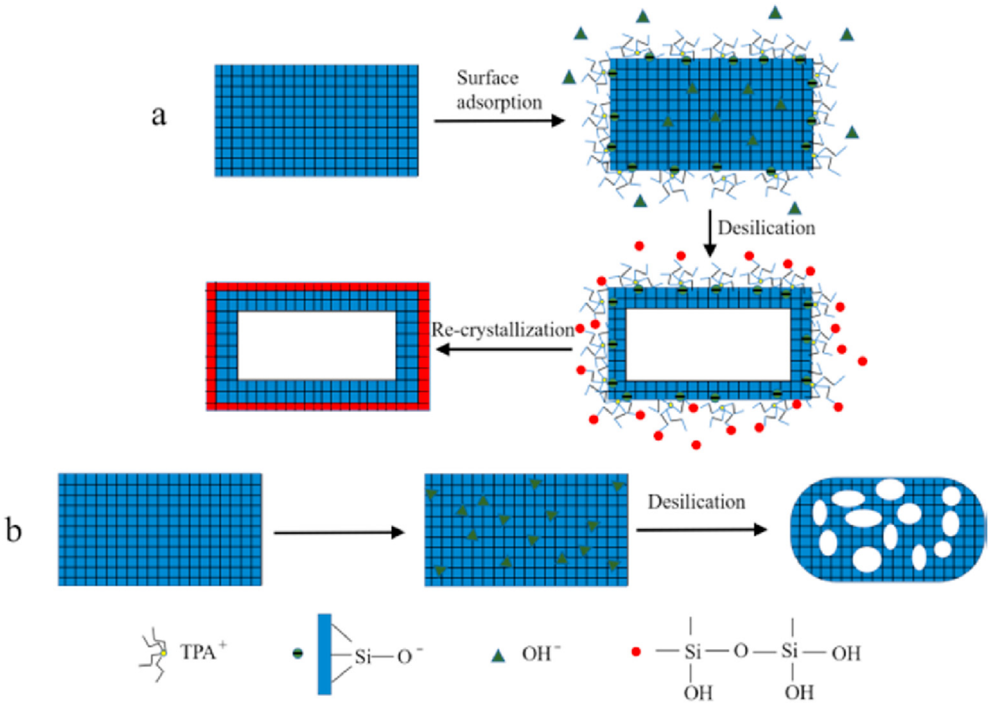

Scheme 1. Mechanism of the alkali treatment and desilication-recrystallization.

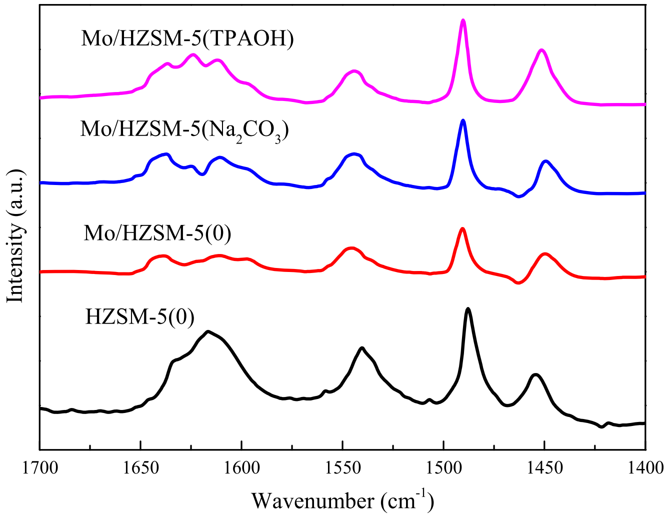

Fig. 7. Py-IR profiles of the different catalysts.

Table 4
The product distributions in the propane aromatization at 5 h over the different catalysts.

Sample	HZSM-5(0)	Mo/HZSM-5(0)	Mo/HZSM-5(Na$_2$CO$_3$)	Mo/HZSM-5(TPAOH)
C_3H_8 conversion x/%	29.74	54.93	67.04	73.01
Product Selectivity s/%				
Methane	14.50	11.29	13.16	9.12
Ethane	5.72	3.25	5.91	2.65
Ethene	12.16	8.83	10.24	8.72
Propene	1.07	2.84	2.10	1.51
Butane	0.50	0.56	0.74	0.43
Butene	0.41	0.35	0.45	0.21
Benzene	21.23	29.21	23.44	34.59
Toluene	32.56	35.49	30.06	31.36
Ethylbenzene	2.98	0.60	3.46	0.63
Xylene	8.87	7.58	10.44	10.78
Aromatic hydrocarbons	65.64	72.88	67.40	77.36

were prone to secondary reactions to form poly-aromatics and coke, leading to the lower aromatics selectivity of Mo/HZSM-5(Na_2CO_3) [41].

In conclusion, Mo/HZSM-5(TPAOH) can enhance propane conversion and aromatics selectivity by the lowest Brønsted/Lewis acid ratio and the hollow structure. Firstly, the coeffect of desilication by OH$^-$ and the protected desilication by TPA$^+$ determined the location of desilication, which ultimately formed the hollow structure to optimize the mass transfer performance [42,43]. Secondly, HZSM-5(TPAOH) with the silicon-rich external surface possessed the higher external surface area, which provided more loading sites for Mo species to generate the Mo-Lewis acid, which decreased the concentration of Brønsted acid, suppressing the side reactions [18]. Assisted by the lower Brønsted/Lewis acid ratio and the hollow structure, the propane aromatization reaction can be efficiently proceeded, achieving a high aromatics selectivity.

Table 3
Adsorption amounts of Bronsted and Lewis acid calculated from Py-IR data.

Sample	Brønsted acid (μmol·g^{-1})	Lewis acid (μmol·g^{-1})	B/L[a]
HZSM-5(0)	228.3	58.9	3.9
Mo/HZSM-5(0)	179.1	86.2	2.1
Mo/HZSM-5(Na_2CO_3)	196.9	72.7	2.7
Mo/HZSM-5(TPAOH)	154.0	123.5	1.3

[a] B/L means the Bronsted/Lewis acid ratio.

3.2.2. *Deactivation behavior of the spent catalysts*

To analyze the nature of the carbonaceous deposits formed in propane aromatization reaction, TG was used to determine the weight loss of the as-used catalysts due to the thermal behavior. Fig. 9 shows TG curves for the spent catalysts and Table 5 lists the coke content of the spent catalysts after the propane aromatization reaction. Two pathways for coke formation in the aromatization reaction, pyrolysis of propane and poly-condensation of formed aromatics [25], were proposed in previous

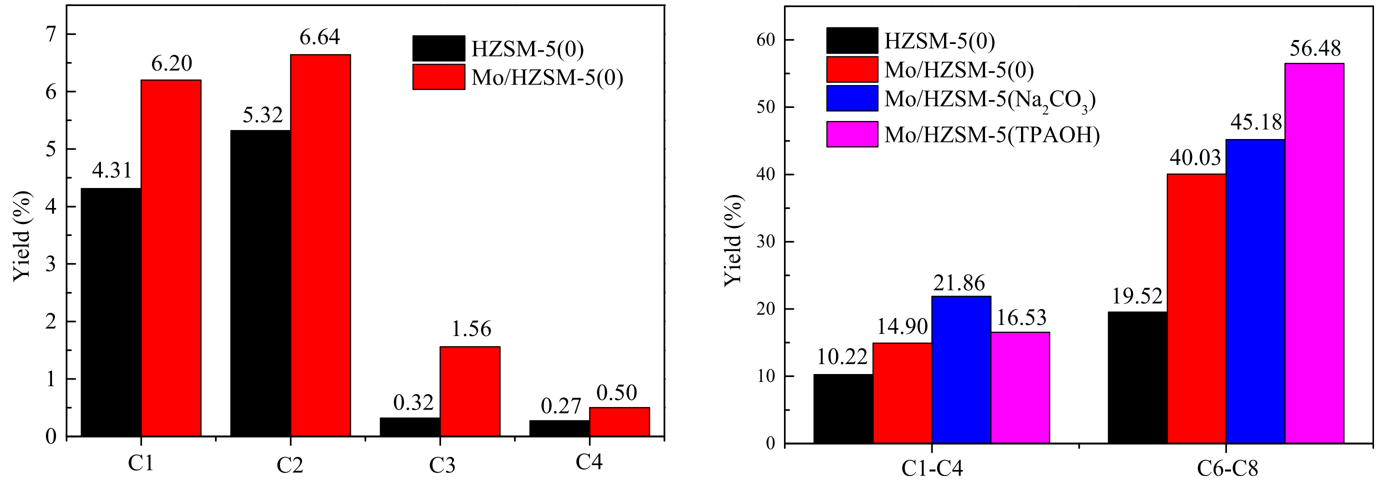

Fig. 8. The product yield in propane aromatization at 5 h over the different catalysts.

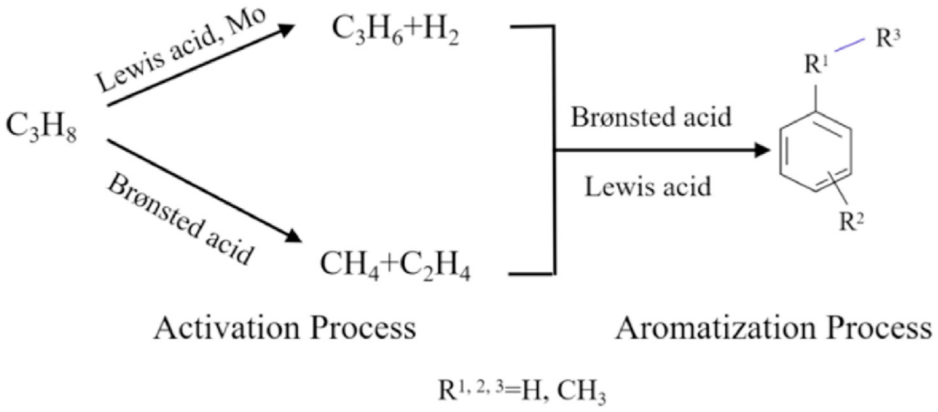

Scheme 2. Mechanism of the propane aromatization recation.

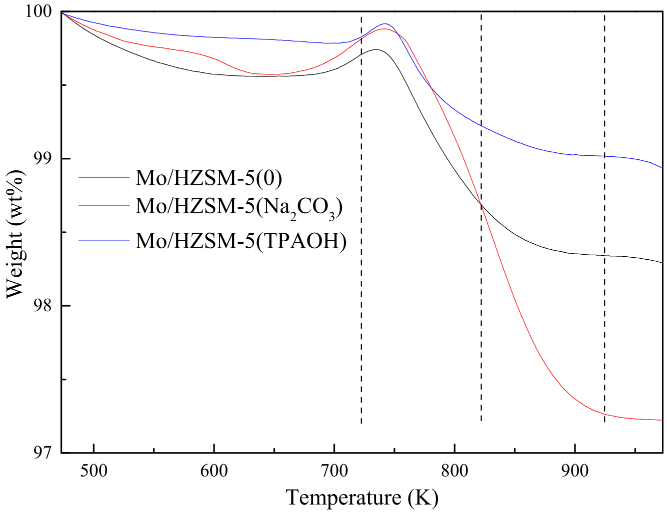

Fig. 9. TG curves of the different catalysts after evaluation.

Table 5
The coke content of the as-used catalysts after 5 h on stream in the propane aromatization reaction.

Sample	C_{total} (10^{-2} g/g_{cat})	C_{soft} (10^{-2} g/g_{cat})	C_{hard} (10^{-2} g/g_{cat})
Mo/HZSM-5(0)	1.36	1.02	0.34
Mo/HZSM-5(Na_2CO_3)	2.52	1.14	1.38
Mo/HZSM-5(TPAOH)	0.81	0.61	0.20

studies [30]. Extensive formation of carbon deposits from the side reactions generally occurred during the aromatization process [27], which blocked the intersections and/or pore mouth of the zeolite, resulting in a severe catalyst deactivation. The main oxidation feature at 723–823 K represents soft coke, which consists of the aliphatic hydrocarbon species and is likely formed in the proximity of Mo species [44]. The other feature, which occurs at 823–923 K, represents hard coke, and belongs to the polynuclear aromatic species, whose formation is catalyzed by Brønsted acid sites [45]. Due to the formation of molybdenum oxide (MoO_3) by MoC_x oxidation above 673 K, an increase for these spent catalysts in weight was detected. Observing the coke content of these spent catalysts, hard carbon deposits gradually increased with the increase of Bronsted acid amount, further demonstrating that the high amount of Bronsted acid was easy to promote the secondary reactions of benzene, deactivating the catalyst. The mass of the spent Mo/HZSM-5(Na_2CO_3) decreased by 1.14 × 10^{-2} g/g_{cat} at 723–823 K, while the spent Mo/HZSM-5(TPAOH) lost only 0.61 × 10^{-2} g/g_{cat}, indicating that the spent Mo/HZSM-5(TPAOH) had fewer aliphatic hydrocarbon [46]. This was due to the fact that the hollow structure was formed by desilication-recrystallization, which accelerated the conversion of intermediate products formed on Mo sites into aromatics [47]. On the contrary, a portion of pore structure of Mo/HZSM-5(Na_2CO_3) was blocked, which was not conducive to the further conversion of intermediate products into aromatics, leading to the formation of a large amount of soft coke on Mo sites. Clearly, the TG profiles showed that there were the weight loss ratio of 1.36% and 2.52% on Mo/HZSM-5 and Mo/HZSM-5(Na_2CO_3), respectively, higher than that of 0.81% over the spent Mo/HZSM-5(TPAOH). Thus, Mo/HZSM-5(TPAOH) effectively inhibited the carbon deposits from the propane aromatization reaction.

3.2.3. The stability of the hollow Mo/HZSM-5(TPAOH) catalyst

Due to the formation of bulky aromatics precursors and the high activity of olefinic intermediates [37], the stability of propane aromatization reaction is a big issue. As showed in Fig. 10, the propane conversions over Mo/HZSM-5(Na_2CO_3) and Mo/HZSM-5(TPAOH) catalysts exhibited a trend of continuous decrease with the extension of propane aromatization reaction time, which was due to the deactivation of the catalysts caused by carbon deposition [4]. In addition, a drop in aromatics selectivity of Mo/HZSM-5(TPAOH) was observed from 74.6% to 56.9% within 48 h on stream, which was much smaller than that within 24 h of Mo/HZSM-5(Na_2CO_3), further demonstrating that the hollow Mo/HZSM-5(TPAOH) can inhibit the carbon deposits and improve the stability of propane aromatization reaction [48].

4. Conclusions

During the desilication-recrystallization of HZSM-5(0), TPA^+ was adsorbed on the external surface of HZSM-5(0) and partly protected the nearby Si species from being etched by OH^-, while the internal Si species were constantly dissolved and leached out. The leached Si species were then recrystallized on the external surface of zeolite under the template of TPA^+ to form a silicon-rich skeleton structure of zeolite. Finally, a regular hollow structured HZSM-5(TPAOH) with a high relative crystallinity was successfully synthesized.

Propane aromatization, as an application reaction, was selected to test the hollow Mo/HZSM-5(TPAOH) catalyst. It was found that the dehydrogenation of propane can be significantly promoted on Mo sites. Mo/HZSM-5(TPAOH) exhibited superior propane conversion of 73.01% and aromatics selectivity of 77.36%, which were higher than those of Mo/HZSM-5(Na_2CO_3) by 5.97% and 9.96%, respectively. The excellent properties of Mo/HZSM-5(TPAOH) catalyst were achieved by the synergetic effect of the lower Brønsted/Lewis acid ratio and excellent mass transfer performance. Additionally, the hollow Mo/HZSM-5(TPAOH) catalyst inhibited the formation of carbon deposits, greatly improving the stability of propane aromatization. The findings in this work can provide a new strategy to synthesize the hollow structured catalysts for enhancing the catalytic properties in propane aromatization, which will give some inspiration to the industrialization development of low-carbon alkanes.

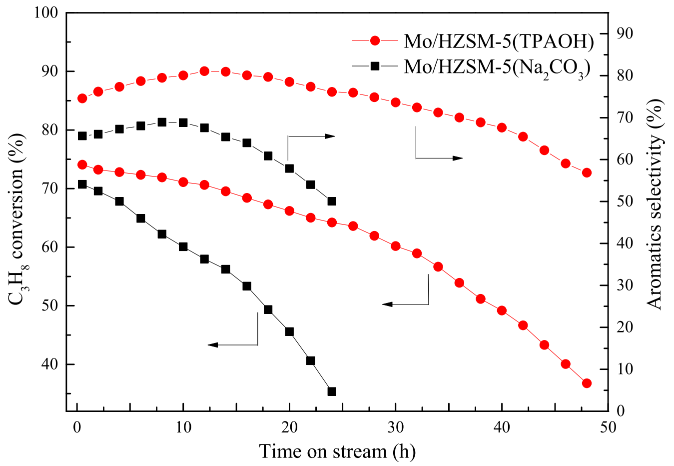

Fig. 10. Durability of Mo/HZSM-5(Na_2CO_3) and Mo/HZSM-5(TPAOH) catalysts in propane aromatization reaction evaluated by a fixed-bed reactor under conditions of 1 atm and 823 K.

CRediT authorship contribution statement

Guohao Xu: Data curation, Writing – original draft. **Peng Zhang:** Methodology, Software. **Junjun Cheng:** Investigation. **Ting Wei:** Sample characterization. **Xuedong Zhu:** Software. **Fan Yang:** Writing – review & editing.

Declaration of competing interest

The authors declare that they have no known competing financial interests or personal relationships that could have appeared to influence the work reported in this paper.

Acknowledgments

This project was sponsored financially by the National Natural Science Foundation of China (No. 21776076).

References

[1] G.G. Oseke, A.Y. Atta, B. Mukhtar, B.J. El-Yakubu, B.O. Aderemi, Increasing the catalytic stability of microporous Zn/ZSM-5 with copper for enhanced propane aromatization, J. King Saud Univ. - Eng. Sci. (2020).
[2] H. Wan, P. Chitta, Catalytic conversion of propane to BTX over Ga, Zn, Mo, and Re impregnated ZSM-5 catalysts, J. Anal. Appl. Pyrol. 121 (2016) 369–375.
[3] I.B. Dauda, M. Yusuf, S. Gbadamasi, M. Bello, A.Y. Atta, B.O. Aderemi, B.Y. Jibril, Highly selective hierarchical ZnO/ZSM-5 catalysts for propane aromatization, ACS Omega 5 (6) (2020) 2725–2733.
[4] M. Raad, S. Hamieh, J. Toufaily, T. Hamieh, L. Pinard, Propane aromatization on hierarchical Ga/HZSM-5 catalysts, J. Catal. 366 (2018) 223–236.
[5] P. He, J. Jarvis, L. Liu, H. Song, The promoting effect of Pt on the co-aromatization of pentane with methane and propane over Zn-Pt/HZSM-5, Fuel 239 (2019) 946–954.
[6] M.A. Abedin, S. Kanitkar, S. Bhattar, J.J. Spivey, Sulfated hafnia as a support for Mo oxide: a novel catalyst for methane dehydroaromatization, Catal. Today 343 (2020) 8–17.
[7] A. Samavati, M. Fattahi, F. Khorasheh, Modeling of Pt-Sn/γ-Al_2O_3 deactivation in propane dehydrogenation with oxygenated additives, Kor. J. Chem. Eng. 30 (1) (2013) 55–61.
[8] F. Babazadeh Shareh, M. Kazemeini, M. Asadi, M. Fattahi, Metal promoted mordenite catalyst for methanol conversion into light olefins, Petrol. Sci. Technol. 32 (8) (2014) 1349–1356.
[9] M.Z. Pedram, M. Kazemeini, M. Fattahi, A. Amjadian, A physicochemical evaluation of modified HZSM-5 catalyst utilized for production of dimethyl ether from methanol, Petrol. Sci. Technol. 32 (8) (2014) 904–911.
[10] C. Mei, Z. Liu, P. Wen, Z. Xie, W. Hua, Z. Gao, Regular HZSM-5 microboxes prepared via a mild alkaline treatment, J. Mater. Chem. 18 (29) (2008).
[11] A. Shahid, N. Ahmed, T. Saleh, S. Al-Thabaiti, S. Basahel, W. Schwieger, M. Mokhtar, Solvent-free biginelli reactions catalyzed by hierarchical zeolite utilizing a ball mill technique: a green sustainable process, Catalysts 7 (12) (2017).
[12] Y. Yang, W. Jiang, J. Jiang, Q. Qiu, P. Mao, M. Wu, L. Zhang, Synthesis of hierarchical ZSM-5 zeolites templated by sodium alginate toward enhanced catalytic activity for esterification, J. Solid State Chem. (2020) 292.
[13] M.M.M. Mostafa, K.N. Rao, H.S. Harun, S.N. Basahel, I.H.A. El-Maksod, Synthesis and characterization of partially crystalline nanosized ZSM-5 zeolites, Ceram. Int. 39 (1) (2013) 683–689.
[14] M. Milina, S. Mitchell, P. Crivelli, D. Cooke, J. Pérez-Ramírez, Mesopore quality determines the lifetime of hierarchically structured zeolite catalysts, Nat. Commun. 5 (1) (2014).
[15] C. Dai, A. Zhang, L. Li, K. Hou, F. Ding, J. Li, D. Mu, C. Song, M. Liu, X. Guo, Synthesis of hollow nanocubes and macroporous monoliths of silicalite-1 by alkaline treatment, Chem. Mater. 25 (21) (2013) 4197–4205.
[16] C. Yang, X. Meng, D. Yi, Z. Ma, N. Liu, L. Shi, Alkali-treatment of silicalite-1/CuY core-shell structure for the adsorption desulfurization of dimethyl disulfide from methyl tert-butyl ether, Ind. Eng. Chem. Res. 58 (4) (2019) 1613–1623.
[17] T. Fu, Z. Ma, Y. Wang, J. Shao, Q. Ma, C. Zhang, L. Cui, Z. Li, Si/Al ratio induced structure evolution during desilication-recrystallization of silicalite-1 to synthesize nano-ZSM-5 catalyst for MTH reaction, Fuel Process. Technol. (2019) 194.
[18] C. Dai, A. Zhang, M. Liu, X. Guo, C. Song, Hollow ZSM-5 with silicon-rich surface, double shells, and functionalized interior with metallic nanoparticles and carbon nanotubes, Adv. Funct. Mater. 25 (48) (2015) 7479–7487.
[19] F. Yang, J. Zhong, X. Liu, X. Zhu, A novel catalytic alkylation process of syngas with benzene over the cerium modified platinum supported on HZSM-5 zeolite, Appl. Energy 226 (2018) 22–30.

[20] C.A. Emeis, Determination of integrated molar extinction coefficients for infrared absorption bands of pyridine adsorbed on solid acid catalysts, J. Catal. 141 (2) (1993) 347–354.

[21] Z. Chen, Z. Li, Y. Zhang, D. Chevella, G. Li, Y. Chen, X. Guo, J. Liu, J. Yu, A green route for the synthesis of nano-sized hierarchical ZSM-5 zeolite with excellent DTO catalytic performance, Chem. Eng. J. (2020) 388.

[22] Z. Ma, T. Fu, Y. Wang, J. Shao, Q. Ma, C. Zhang, L. Cui, Z. Li, Silicalite-1 derivational desilication-recrystallization to prepare hollow nano-ZSM-5 and highly mesoporous micro-ZSM-5 catalyst for methanol to hydrocarbons, Ind. Eng. Chem. Res. 58 (6) (2019) 2146–2158.

[23] D. Verboekend, J. Pérez-Ramírez, Design of hierarchical zeolite catalysts by desilication, Catal. Sci. Technol. 1 (6) (2011).

[24] W. Zhu, Z. Chen, Y. Pan, R. Dai, Y. Wu, Z. Zhuang, D. Wang, Q. Peng, C. Chen, Y. Li, Functionalization of hollow nanomaterials for catalytic applications: nanoreactor construction, Adv. Mater. 31 (38) (2019) e1800426.

[25] M. Raad, A. Astafan, S. Hamieh, J. Toufaily, T. Hamieh, J.D. Comparot, C. Canaff, T.J. Daou, J. Patarin, L. Pinard, Catalytic properties of Ga-containing MFI-type zeolite in cyclohexane dehydrogenation and propane aromatization, J. Catal. 365 (2018) 376–390.

[26] P. Zhu, G. Yang, J. Sun, R. Fan, P. Zhang, Y. Yoneyama, N. Tsubaki, A hollow Mo/HZSM-5 zeolite capsule catalyst: preparation and enhanced catalytic properties in methane dehydroaromatization, J. Mater. Chem. 5 (18) (2017) 8599–8607.

[27] C.H.L. Tempelman, E.J.M. Hensen, On the deactivation of Mo/HZSM-5 in the methane dehydroaromatization reaction, Appl. Catal. B Environ. 176–177 (2015) 731–739.

[28] C.H.L. Tempelman, V.O. de Rodrigues, E.R.H. van Eck, P.C.M.M. Magusin, E.J.M. Hensen, Desilication and silylation of Mo/HZSM-5 for methane dehydroaromatization, Microporous Mesoporous Mater. 203 (2015) 259–273.

[29] C. Peng, Z. Liu, Y. Yonezawa, Y. Yanaba, N. Katada, I. Murayama, S. Segoshi, T. Okubo, T. Wakihara, Ultrafast post-synthesis treatment to prepare ZSM-5@Silicalite-1 as a core-shell structured zeolite catalyst, Microporous Mesoporous Mater. 277 (2019) 197–202.

[30] Y. Song, Y. Xu, Y. Suzuki, H. Nakagome, Z.-G. Zhang, A clue to exploration of the pathway of coke formation on Mo/HZSM-5 catalyst in the non-oxidative methane dehydroaromatization at 1073K, Appl. Catal. Gen. 482 (2014) 387–396.

[31] M. Rahman, A. Sridhar, S.J. Khatib, Impact of the presence of Mo carbide species prepared ex situ in Mo/HZSM-5 on the catalytic properties in methane aromatization, Appl. Catal. Gen. 558 (2018) 67–80.

[32] K. Velebná, M. Horňáček, V. Jorík, P. Hudec, M. Čaplovičová, L.u. Čaplovič, The influence of molybdenum loading on activity of ZSM-5 zeolite in dehydroaromatization of methane, Microporous Mesoporous Mater. 212 (2015) 146–155.

[33] T. Fu, R. Qi, X. Wang, W. Wan, Z. Li, Facile synthesis of nano-sized hollow ZSM-5 zeolites with rich mesopores in shell, Microporous Mesoporous Mater. 250 (2017) 43–46.

[34] Z. Wang, Q. Sun, D. Wang, Z. Hong, Z. Qu, X. Li, Hollow ZSM-5 zeolite encapsulated Ag nanoparticles for SO_2-resistant selective catalytic oxidation of ammonia to nitrogen, Separ. Purif. Technol. 209 (2019) 1016–1026.

[35] T. Fu, R. Qi, W. Wan, J. Shao, J.Z. Wen, Z. Li, Fabrication of hollow mesoporous nanosized ZSM-5 catalyst with superior methanol-to-hydrocarbons performance by controllable desilication, ChemCatChem 9 (22) (2017) 4212–4224.

[36] H. Liu, W. Shen, X. Bao, Y. Xu, Methane dehydroaromatization over Mo/HZSM-5 catalysts: the reactivity of MoC_x species formed from MoO_x associated and non-associated with Brönsted acid sites, Appl. Catal. Gen. 295 (1) (2005) 79–88.

[37] W. Zhou, J. Liu, L. Lin, X. Zhang, N. He, C. Liu, H. Guo, Enhanced dehydrogenative aromatization of propane by incorporating Fe and Pt into the Zn/HZSM-5 catalyst, Ind. Eng. Chem. Res. 57 (48) (2018) 16246–16256.

[38] X. Gao, L. Zhang, Z. Tao, H. Chen, Y. Zhang, H. Gong, X. Wen, Y. Yang, Y. Li, New insight into seeding process leading to improved zeolitic acidity and surface properties for its catalytic application in propane aromatization, Catal. Today (2020).

[39] Y. Song, Q. Zhang, Y. Xu, Y. Zhang, K. Matsuoka, Z.-G. Zhang, Coke accumulation and deactivation behavior of microzeolite-based Mo/HZSM-5 in the non-oxidative methane aromatization under cyclic CH_4-H_2 feed switch mode, Appl. Catal. Gen. 530 (2017) 12–20.

[40] Y. Xu, J. Liu, J. Wang, G. Ma, J. Lin, Y. Yang, Y. Li, C. Zhang, M. Ding, Selective conversion of syngas to aromatics over Fe_3O_4@MnO_2 and hollow HZSM-5 bifunctional catalysts, ACS Catal. 9 (6) (2019) 5147–5156.

[41] C. Karakaya, R.J. Kee, Progress in the direct catalytic conversion of methane to fuels and chemicals, Prog. Energy Combust. Sci. 55 (2016) 60–97.

[42] Z. Jian, L.U.O. Wen, Y.A.N. Kai, S.U.N. Li-Li, Hollow ZSM-5 zeolite microspheres with improved adsorption and catalytic properties, J. Inorg. Mater. 31 (8) (2016).

[43] N. Chu, J. Wang, Y. Zhang, J. Yang, J. Lu, D. Yin, Nestlike hollow hierarchical MCM-22 microspheres: synthesis and exceptional catalytic properties, Chem. Mater. 22 (9) (2010) 2757–2763.

[44] J.J. Spivey, G. Hutchings, Catalytic aromatization of methane, Chem. Soc. Rev. 43 (3) (2014) 792–803.

[45] A. Sridhar, M. Rahman, S.J. Khatib, Enhancement of molybdenum/ZSM-5 catalysts in methane aromatization by the addition of iron promoters and by reduction/carburization pretreatment, ChemCatChem 10 (12) (2018) 2571–2583.

[46] N. Kosinov, E.A. Uslamin, L. Meng, A. Parastaev, Y. Liu, E.J.M. Hensen, Reversible nature of coke formation on Mo/ZSM-5 methane dehydroaromatization catalysts, Angew Chem. Int. Ed. Engl. 58 (21) (2019) 7068–7072.

[47] K. Wang, X. Huang, D. Li, Hollow ZSM-5 zeolite grass ball catalyst in methane dehydroaromatization: one-step synthesis and the exceptional catalytic performance, Appl. Catal. Gen. 556 (2018) 10–19.

[48] Y. Wu, J. Li, Y. Chai, H. Guo, C. Liu, Synergetic effect of H-ZSM-5/Silicalite-1@Pt/Al_2O_3 core-shell catalyst to enhance the selective hydrogenation of p-xylene, J. Membr. Sci. 496 (2015) 70–77.